DOI: 10.21917/ijsc.2026.0561

IMREN2UNET - IMPROVED RES-NNU-NET MODEL FOR LESION SEGMENTATION WITH FCD

Alok Kumar[1] and N. Mahendran[2]

[1]*Department of Computer Science and Engineering, Government College of Engineering, Dharmapuri, India*
[2]*Department of Electronics and Communication Engineering, M. Kumarasamy College of Engineering, India*

Abstract

Focal Cortical Dysplasia (FCD) is a common disorder causing drug-resistant seizures and it is usually managed surgically. The precise segmentation of lesions from MRI and other neuroimaging data is important to diagnose and plan surgery accurately. Typical U-Net models cannot capture the significant textures, irregular shapes, and delicate boundaries of FCD lesions. To alleviate these limitations, we introduce an advanced deep-learning model called ImReN2UNET that addresses FCD universal lesion segmentation using a GLCM-based loss function and improved residual block architecture. The introduction of GLCM-based loss function sharpens model localization and delineation by emphasizing textural features and spatial interdependence in lesions. This is a significant improvement in this field because identifying minute and complex lesions is of the utmost importance in medical imaging. The ImReN2UNET architecture runs on the robust presence of the nn-U-Net architecture and combines residual learning with texture information to segment the FCD lesion regions. The proposed method yields considerably more precise and reliable lesion segmentation by experimental comparisons against state-of-the-art segmentation techniques. This technique provides a powerful instrument for the diagnosis and assessment of FCD and thus informs clinical decisions for better outcomes for the patients.

Keywords:

FCD, Residual, Neural Network, Loss Function, GLCM

1. INTRODUCTION

Currently, data from around the globe reveal that nearly 70 million people suffer from epilepsy [1]. Some of the primary reasons affecting some patients with drug-resistant epilepsy are Focal Cortical Dysplasia (FCD) [2]. A minimum of 70% of patients with lesion excision for FCD have seizure-free outcomes, making it the most effective intervention for DREFCD [3]. For such interventions to be effective, localization and segmentation of FCD lesions are very crucial. Nevertheless, there still exist several hurdles to diagnosing FCD lesions in clinical settings.

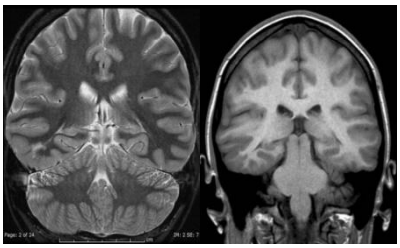

Fig.1. FCD lesion on MRI of two patients

Since they are comparatively subtle, it becomes quite easy to overlook any structural changes linked to FCD on MR images, thus benefiting and passing unnoticed in regular visual assessments. Examples of such abnormalities are hyperintense signals on T2-weighted or FLAIR sequences, the transmantle sign, abnormal sulcal or gyral patterns, cortical thickening, and blurring of the gray-white matter junction [4].

The Fig.1 shows about a one-third of patients with FCD do not show lesions on MRI [5], which makes it quite difficult for the clinician further to segment the locations of the lesions and make their evaluations. Notwithstanding these challenges, the need for methods that assist a computer to help fully and automatically determine FCD lesions is urgent and holds the utmost value.

In medical image analysis, DL-based approaches have become the state-of-the-art approach due to the growth of DL and the success of convolutional neural networks particularly [6, 8, 9, 11]. Biomedical image segmentation challenges have shown promising outcomes with U-Net-based networks being the most effective DL segmentation solution [11]. The U-Net is a fully convolutional encoder-decoder type network [10]. On the other hand, DL-based segmentation relies on several additional elements and the hyperparameters of the neural network training pipeline, including dataset preparation, image augmentation methods, training batch size, and so on [8]. Low efficiency is caused by choosing components that are not ideal for the training pipeline, and this design relies on the dataset. To solve the problem of choosing training pipeline components optimally without human intervention or trial and error, Isensee et al. [46] created the nnUNet framework. When applied to a segmentation task, the nnUNet automatically configures the whole training pipeline, including dataset attributes and hardware restrictions. It is a completely automatic and adaptable framework. Standard convolutional blocks make up the nnUNet's U-Net type architecture, which is self-configuring in terms of topology (network depth, kernel sizes, and pooling operations). The network uses deep supervision, though does not have architectural features observed more advanced U-Net type architectures, such as residual, dense, or inception blocks [46], [11]. In terms of overall performance, the nnUNet was at the top of its class for 33 out of 53 anatomical structures [46]. The use of a systematic approach to adapting the configuration of the training pipeline to new datasets is largely responsible for nnUNet's outstanding performance, not a complex U-Net design [7]. Despite using a very basic U-Net design, the approach outperformed the state-of-the-art on many datasets.

This research work found that by combining nn-U-Net with the GLCM-based loss function generated residual block, they could provide expert segmentation results that were highly focused on the defective region. Our particular contributions are outlined below:

- Segmenting the impacted region using a residual-guided U-Net.
- To further reduce the texture error and improve the pixel-wise precision, the GLCM may be used as an auxiliary loss

function to direct the development of spatially correct texture.

- Conserving time and reducing unnecessary human intervention by automatically producing the ground truth needed to train the segmentation model using a defect masking approach.
- Greater success in segmenting FCD lesions with complex and difficult textures.
- The benefits of incorporating texture-aware methods into nn-U-Net are demonstrated.
- Possible uses for GLCM-based methods in medical imaging applications.

This paper is organized as follows. Interrelated works are detailed in Section 2. Section 3 provides a detailed description of the proposed model's design and characteristics. The experimental process and its outcomes are detailed in Section 4. Section 5 concludes the study with its results and recommendations for further study.

2. LITERATURE REVIEW

In the last few decades, voxel-based morphometry (VBM) [48] and surface-based morphometry (SBM) [13] have been used in the effort of computer-assisted identification of FCD lesions. Images are first registered to standardize their location in space and attain voxelwise alignment as part of the VBM process [14,49]. Then, voxel-wise statistical analysis is performed.[12]. Voxelwise classification is a trainable task for machine learning models [16,17]. The use of non-linear registration can change local cortical architecture and cause detection failures in VBM approaches, which are already sensitive to image registration as well as individual brain variation. Alternatively, SBM approaches to reconstruct the brain's surface to extract information unique to each vertex, including its thickness, curvature, sulcal depth, and so-called "doughnut" attributes. To detect anomalous vertex clusters, machine learning models are developed using these vertex attributes for vertex-wise classification [18,20]. Because they need to recreate the cortex's surface, which might take several hours per patient, SBM approaches are computationally intensive, yet they are good at identifying FCD. Both VBM and SBM depend on low-level characteristics that are hand-crafted, which means they cannot be discriminative enough to distinguish between normal structures and FCD lesions.[28]. Recent developments in AI theory and parallel computing have created exciting new possibilities for the use of deep learning methods, in particular convolutional neural networks (CNNs), in the medical field [21]. Recently, MR images of FCD lesions have been detected using CNNs [22]. A voxel-wise classification issue, as described in [23-25], may be used to create the identification of FCD lesions. Many medical segmentation tasks have made use of fully convolutional networks like UNet [26] and its derivatives, such as Attention-UNet [27] and Multi-Res-UNet [47], because of their ability to efficiently provide dense predictions from start to end. Before its extension to 3D Res-UNet with residual convolution blocks [30], the UNet was trained to identify FCD lesions using FLAIR slices [29]. A significant increase in performance was achieved by making use of the additional data included inside the 3D patches. Incorporating MultiResUNet with attention gating, the Multi- Multi-Res-Attention-UNet improves the UNet [31]. Its purpose is to identify important characteristics that stand in for complicated FCD lesions.

2.1 U-NET ARCHITECTURE

When U-Net [50] was introduced in 2015, the encoder-decoder-like structure quickly established the gold standard in biomedical segmentation. U-Net design uses an encoder route to progressively decrease the resolution of space by half and double the number of feature maps to extract significant semantic and global information. To restore the spatial resolution, the decoder reduces the attribute maps in half while progressively doubling the spatial resolution.[32]. The finer details of the encoder and the course aspects of the decoder are combined in skip connections. A 2D U-Net optimized with soft dice loss was suggested by Dong et al. [33] to address the imbalance in the BraTS 2015 dataset. Their approaches enhanced segmentation performance by using substantial data augmentation techniques. The winner of BraTS 2018, Myronenko [34], suggested an encoder-decoder network that could extract more deep features using an asymmetrically more substantial encoder. The shared encoder is regularized using their method's variational autoencoder branch. The author found that performance was enhanced when the network width was increased. Their method uses typical convolutions and large input patch sizes, which makes it computationally costly. A 3D architecture similar to U-Net was created by Insensee et al. [35]. It was trained using enormous patch size, dice loss, with a lot of data augmentation. To further increase gradient transmission to lower levels, deep supervision was used. To enhance the flow of information, Li et al. [36] suggested an up-skip link between the encoder and decoder. They used a cascade training technique and an inception module in their network to successively segment tumor locations. When it came to training and general DCNNs for 3D brain tumor segmentation, Zhao, Y. et al. [37] examined several techniques for processing data, building models, and optimizing them. Their approach placed second in the BraTS 19 Challenge.

2.2 CHALLENGES AND SOLUTIONS

Subtle brain lesions caused by Focal Cortical Dysplasia (FCD) pose formidable obstacles to precise detection and segmentation owing to their complicated textures and small intensity contrasts. An advanced approach is the nn-U-Net, whose performance is limited owing to the dependence on a range of simplified intensity and structural information from training. This opens a way towards the development of an optimal approach that will merge between classical deep learning approaches and texture-based conclusions in particular. The advantage will be that segmentation is carried out with precision and robustness, particularly for the cases associated with subtle- and heterogeneous-texture differences that occur in FCD lesions. Implementation and initial trials of this new approach are viewed as challenges toward its applicability on different datasets and clinical situations while providing texture awareness.

3. PROPOSED SYSTEM

An advanced residual neural network (ResNet), which includes a Gray Level Co-occurrence Matrix (GLCM) loss function, combined with a U-Net architecture, is proposed in this

work; this will assist in achieving more accurate FCD segmentation in medical images.

The model aims to offer greater accuracy and precision when segmenting individual lesion regions in FCD by leveraging techniques to address some complex challenges in medical image analysis. ResNet allows for deeper layers, dampening the vanishing gradient effect.

The model can learn more features without a fall in performance. The loss function GLCM would help incorporate the spatial texture information, thus enhancing the model's capacity to discriminate minor differences in tissue properties, which is important for the very accurate identifying of lesion areas in FCD.

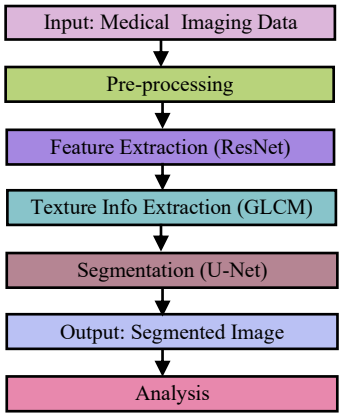

Fig.2. Implementation flow diagram of Proposed model

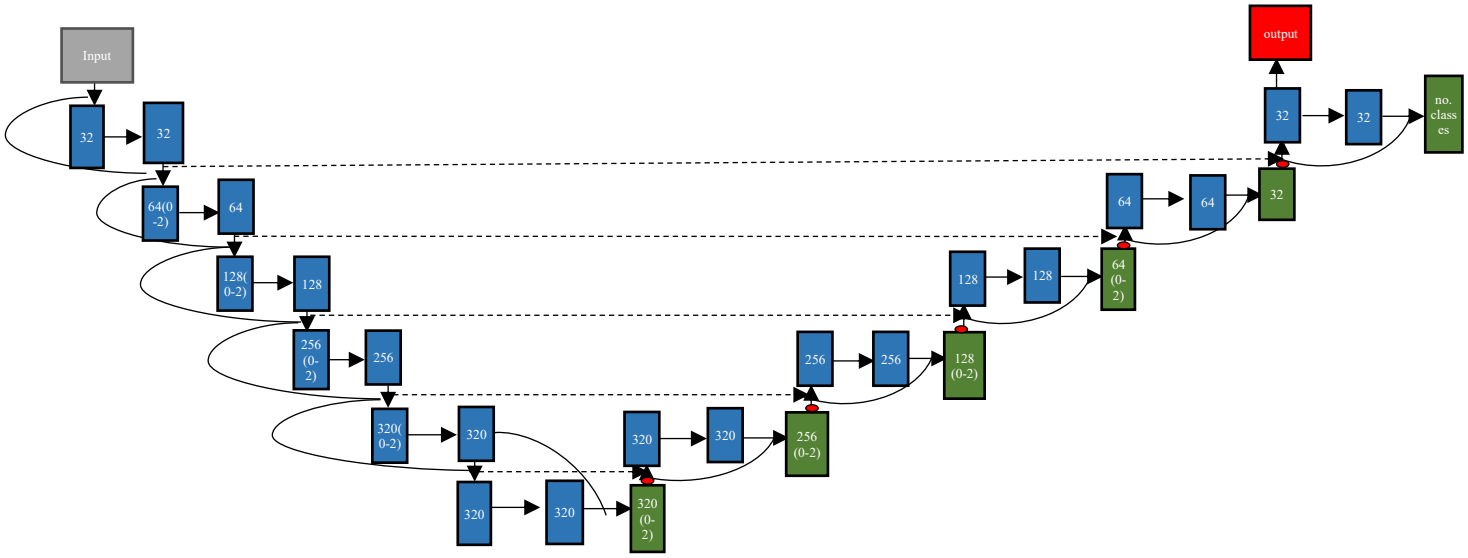

Fig.3. Residual U-Net Architecture

U-Net architecture has been known to be very effective in image segmentation tasks; it allows the identification and delineation of boundaries in medical imaging where fine details have to be taken into account [15]. The remaining parts in this proposed model enhance the extraction process in the model during the segmentation. An expected comparison of this proposed framework with conventional methods will enable it to achieve better outcomes in lesion segmentation in FCD, thus allowing more accurate diagnosis and treatment plans. Fig.2 presents the overall implementation flow of the proposed model, and through this, the data exchange and sequence network steps for attaining the ultimate performance in segmentation can be easily visualized.

3.1 IMPROVED RESIDUAL NN

Residual-nnUNet incorporates a completely residual UNet into the design of nnUNet, expanding upon the work of ResNet [39]. As seen in Fig.3's template, this results in the proposal of Residual-nnUNet, which incorporates residual connections at the depth level. By enabling the network to keep information from prior layers, the residual link enables the addition of the input to the output of a convolutional block. To solve the vanishing gradient problem and improve gradient flow during backpropagation, this approach has been suggested to improve deep network training.

3.2 GLCM BASED TEXTURE FEATURE EXTRACTION

The Grey Level Co-occurrence Matrix serves to characterize the texture of an FCD image through the computation of the frequency of pixel pairs that may exhibit spatial relationships within specified regions of interest. In the analysis of a specific image characterized by N grey levels, one constructs a NxN co-occurrence matrix P. Within this matrix, the entry at position (i,j) represents the frequency with which grey level i is spatially associated with grey level j. An illustration of spatial relationship configuration in an image of dimensions (N_x,N_y) may involve all coordinates of (x,y) and $(x+1,y)$, representing their horizontal adjacency. The value at location (i,j) in P represents the cumulative count of instances where grey level i and grey level j are found in horizontal adjacency within the image. The GLCM, by focusing on the spatial distribution of pixel values rather than directly comparing spatially matching pixel values, serves as an effective measure of texture similarity that complements the pixel-by-pixel similarity metric known as PSNR.

Typically, a variety of GLCMs are generated, incorporating a comprehensive range of spatial relationships to thoroughly define the texture of an image. In addition to the standard $(x;y)$ to $(x+1,y)$ relationship, the offset value can be extended to encompass an omnidirectional pixel distance $d \in Z$, thereby allowing for spatial

relationships to be expressed as (*x,y*) to (*x+dx,y+dy*). This study employs GLCMs calculated in eight directions, incorporating a 45-degree offset, extending to a distance of up to 10 pixels, and utilizing a 4-bit precision, resulting in 16 grey levels following quantization. This yields a tensor *P* with dimensions 8x10x16x16, resulting in 80 individual 16x16 GLCMs, each corresponding to a specific spatial relationship configuration. The raw transformation is subject to analysis for various statistical measures, and a pixelwise comparison can be conducted on GLCMs across different images to quantitatively assess texture similarity in a comparative manner. When a generated super-resolution image exhibits textural similarities to the original high-resolution image, it is predicted that the associated gray-level co-occurrence matrices will demonstrate proximity in terms of L1 or L2 distances. The computation of the L1-GLCM error is expressed in Eq.(1):

$$\mathrm{GLCM}_{\mathrm{Loss}} = \frac{\sum_{i,j} | \bar{P}_{SR}(i,j) - \bar{P}_{\mathrm{HR}}(i,j)|}{\sum_{i,j} ij} \quad (1)$$

3.3 IMPROVED RESIDUAL NETWORK WITH GLCM LOSS FUNCTION

The architecture employed in this investigation is the Residual neural network, which draws upon the U-net architecture [39]. The model employs Parametric Rectified Linear Units (PReLU) for its activation functions, while batch normalization layers have been eliminated due to their negative impact on super-resolution convergence. The Fig.4 illustrates Generator *G*. The L1 pixel-wise loss was employed due to its superior performance in SRCNN convergence and its ability to mitigate severe smearing when contrasted with the L2 loss, as it diminishes the penalty associated with high-frequency noise and texture. Model G went through training for a total of 100,000 iterations, utilizing cropped mini-batches sized at 16x192x192. The optimization procedure was executed employing the Adam optimizer, with the learning rate set at $1e^{-4}$. Generator *G* demonstrates the ability to enhance image resolution and refine medium to large-scale features. Res-Unet is optimized to produce high-frequency features and textures that are less than three to five pixels. The Res-nnUnet integrates *G* with a discriminator *D*, as illustrated in Fig.5, through the adversarial loss known as ADV Loss. The joint training process is set to extend for an additional 150,000 iterations. In addition to L1Loss and ADV Loss, the overall generator loss incorporates the VGG-19 perceptual objective and the newly introduced GLCM Loss (refer to Eq.(1)). The total generator loss is defined in Eq.(2):

$$G_{\mathrm{Loss}} = L_{1\_\mathrm{Loss}} + \alpha VGG_{19\_\mathrm{Loss}} + \beta \mathrm{ADV}_{\mathrm{Loss}} + \gamma \mathrm{GLCM}_{\mathrm{Loss}} \quad (2)$$

The parameters a, b, and c are defined as scaling terms with values of 1e-5, 1e-3, and 1e-4, respectively, to ensure that their magnitudes remain comparable to the L1 loss.

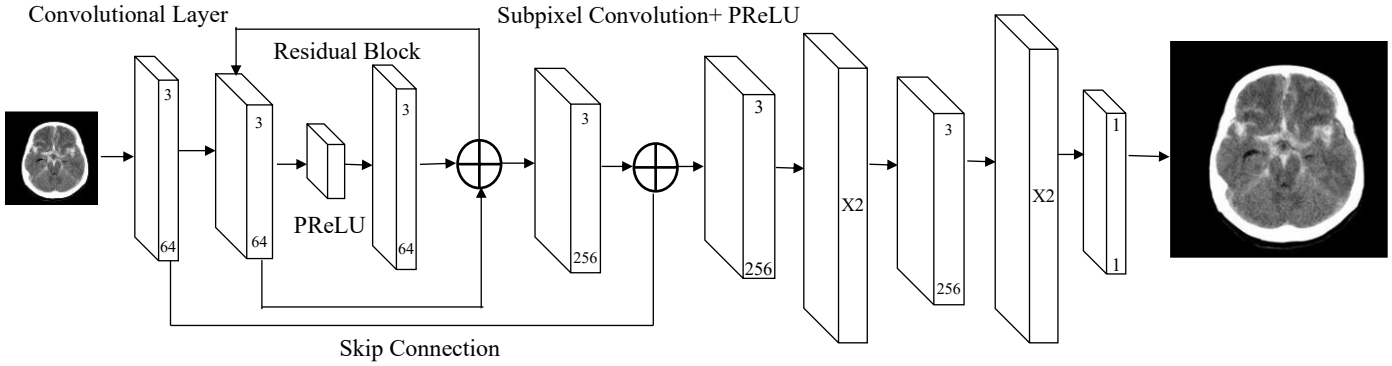

Fig.4. Architecture of the Improved Residual Neural Network U-Net Model (ImReN2UNET)

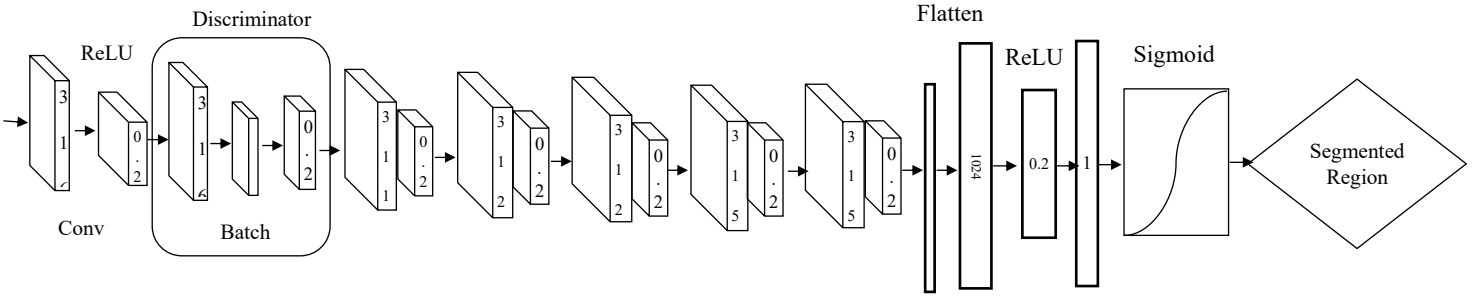

Fig.5. The structural design of the Discriminator network

3.4 IMREN2UNET SEGMENTATION

The proposed model-based segmentation technique is detailed in this section. The Fig.6 provides a detailed illustration of the description. This image presents a comparison between a conventional convolutional block and a residual block, emphasizing the advancements introduced by ResNet architectures. The conventional block (a) implements sequential convolutional and ReLU operations, converting input x into output y. The residual block (b) incorporates a shortcut connection, enabling the input x to skip the convolutional layers and be directly summed with the output of the residual branch (x). The design, articulated as $y = F(x) + x$, serves to address the vanishing gradient issue, facilitating the training of more complex

networks through the retention of original information and enhancement of gradient propagation. Residual blocks play a significant role in facilitating efficient and stable learning processes within very deep neural networks.

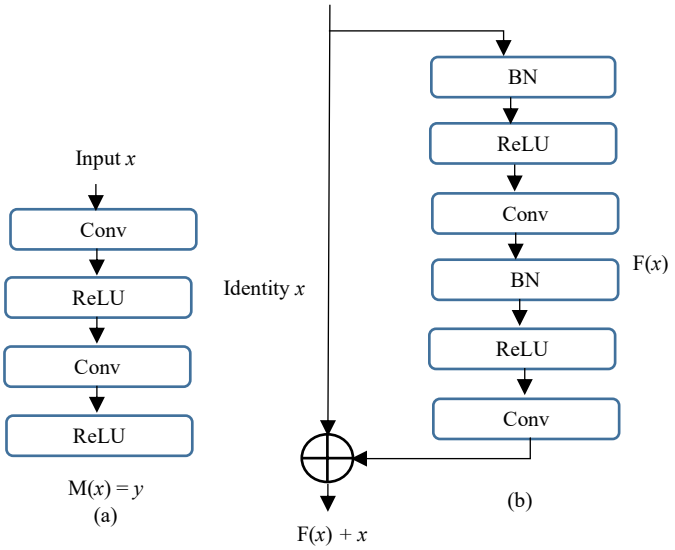

Fig. 6. A basic component of neural networks, as seen in Fig.5. (a) U-Net takes use of a traditional feed-forward neural network, and (b) Residual U-Net uses an identity map as its residual unit

In both the encoder and decoder routes, there are four stages, and each step has a residual block. Every step of the encoder route is considered an independent unit, and there are repeating units inside each step. On the first stage, there are three units. There are a total of four units in the second stage and six in the third stage. There are three units in the last level.

Including the fast link that goes through the convolutional layer, the encoder path has a total of 50 convolutional layers. Every block performs a convolution process. After scaling the input image to 128×128 dimensions, batch normalization is applied to the resulting batch. After batch normalization is applied, a 2D convolution with a 3×3 filter is performed.

Adopting a Residual U-Net—composed of an up-sampling layer, a concatenation layer, a succession of convolutional layers, batch normalization, and ReLU activation functions—defines the decoder path. The main advantage of using an Up Sampling layer is that it may create a dense activation map while retaining the original activation dimensions. When up-sampling, transpose convolution is used. Following the use of a sigmoid activation function, a 1×1 convolutional layer is used. The proposed model's probability score is generated using the sigmoid activation function. The layer is then transformed into the segmentation map as desired using features from a single channel.

4. RESULT AND DISCUSSION

We used two main metrics: evaluations at the subject level and assessments at the voxel level. On an individual level, we made use of detection sensitivity (sSens) and the mean false-positive cluster count (nFPC). Following the criteria outlined in [40], an FCD lesions was determined to be discovered if the prediction and ground truth overlapped by at least one voxel. The following Eq.(3) is the definition of sSens:

$$\text{sSens} = \frac{TP_s}{TP_s + FN_s'} \tag{3}$$

True positive subjects are represented by TPs, whereas false negative subjects are represented by FNs. The number of false-positive lesion detections in FCD patients is quantified by nFPC. Clusters are originally defined using voxel connectivity analysis; a false-positive cluster is one that does not include any real lesion voxels. The generally used measures of sensitivity (Sens), precision (Prec), and the dice coefficient (DC) were used for assessment at the voxel level. These measures are described in Eq.(4) – Eq.(6):

$$\text{Prec} = \frac{TP}{TP + FP'} \tag{4}$$

$$\text{Sens} = \frac{TP}{TP + FN'} \tag{5}$$

$$\text{DC} = \frac{2 \times TP}{2 \times TP + FN + FP'} \tag{6}$$

where TP is the count of voxels that are true positives, FP is the count of voxels that are false positives, and FN is the count of voxels that are false negatives.

4.1 RESULTS

An experiment series was carried out to verify the efficacy of our proposed model. For this purpose, we used a number of state-of-the-art CNN models that have been used for segmenting FCD lesions before, such as Attention-UNet [41], Res-UNet [42], and Multi-Res-Attention-UNet [43]. The comparison study also includes transformer-based models, namely UNETR [44] and its enhanced version, UNETR++ [45].

4.2 EVALUATATION OF VARIOUS MODELS

4.2.1 Quantitative Comparisons:

Each patient in the test set performed examinations at both the subject and voxel levels. Connected component analysis was used on the segmentation masks to detect and classify different clusters in order to measure nFPC. Clusters were categorized as FPCs if they did not intersect with the ground truth. The outcomes for the FCD lesion segmentation tests are in Table.1. The Table.2 also shows the total number of true positive lesions, false negative lesions, and false positives.

Table.1. Performance Comparison on Various Models

Methods	nFPC	sSens	Sens	DC	Prec
Attention-UNet [21]	1.118 ±1.906	0.647	0.246 ±0.258	0.236 ±0.268	0.336 ±0.359
UNETR [30]	1.529 ±2.304	0.588	0.115 ±0.171	0.115 ±0.171	0.344 ±0.399
Multi-Res-Attention-UNet [25]	3.000 ±3.597	0.471	0.228 ±0.314	0.187 ±0.262	0.219 ±0.307
UNETR [31]	0.882 ±0.900	0.706	0.436 ±0.340	0.373 ±0.295	0.382 ±0.321
ImReN2UNET (ours)	0.158 ±0.298	0.869	0.537 ±0.368	0.475 ±0.109	0.527 ±0.354

Table.2. Comparison of the number of TP, FP and FN Lesion among different Models

Methods	FP lesions	TP lesions	FN lesions
Attention-UNet [21]	19	11	6
UETR [30]	26	10	7
Multi-Res-Attention-UNet [25]	51	8	9
Rs-UNet [24]	21	13	4
UNTR + + [31]	15	12	5
Proposed Model (ours)	3	14	3

4.2.2 Qualitative Comparisons:

The Fig.7 shows the segmentation results from a single typical instance for a qualitative comparison of FCD lesion segmentation. It provides three axial slices that overlap with each other and various model prediction maps. A better perspective is achieved by enlarging the ROI enclosing the lesion and the prediction map. Compared to competing models, the proposed one obtained a higher DC of 0.898.

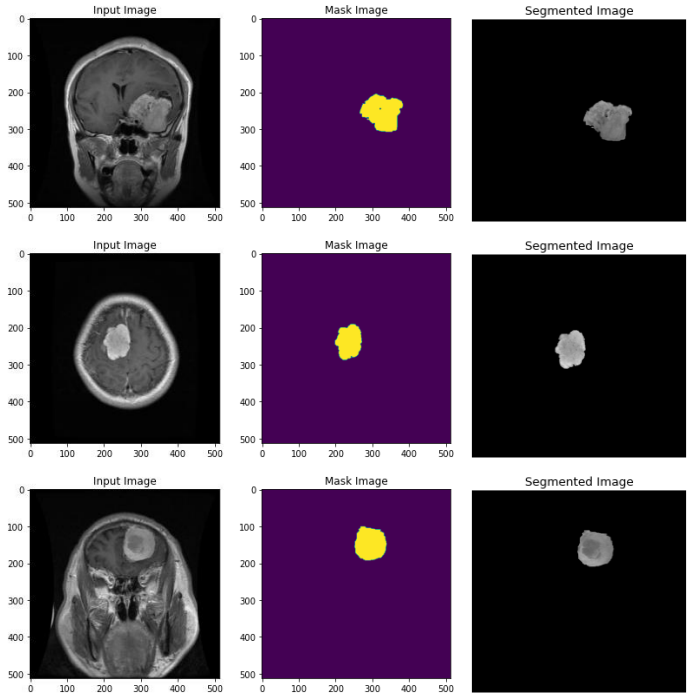

Fig.7. Segmentation outcomes of a single Image

4.3 Ablation studies

The impact of model architecture on performance was investigated via the use of experiments. At first, we set out to evaluate the efficacy of models trained with different input sequences, as T1 and FLAIR imaging give different perspectives on the structural changes associated with FCD lesions. Table 3 provides a more comprehensive summary of the assessment results.

To verify the enhanced performance offered by various self-attention techniques, we performed several studies. For our research, we swapped out the DSA module for the SSA and CSA modules in the proposed design and ran the same tests. Table 4 shows the results of comparing models with various self-attention modules. For transformer-based models to extract useful semantic characteristics, the patch size is crucial. We ran tests using MS-DSANET and different patch sizes to see how they affected segmentation speed. Table 5 details the performance comparisons of these various patch sizes.

4.3 LOSS FUNCTION ANALYSIS

This section shows the results and analyses of the ImReN2UNET network performance, when trained with GLCM metric. The first set of experiments illustrate GLCM performance as a metric to quantify texture accuracy of the network in its standard configuration with the VGG19 loss function. Then setup gets extended to using GLCM as an auxiliary loss function as shown in Equation 2.

Instead of using the conventional VGG loss function in the ResNet network, the GLCM metric may be directly employed as a loss function since it quantifies and delineates texture accuracy. Here, the GLCM is computed using floating point precision to keep differentiability, and it is computed with a 2px offset in 8 directions to keep computational speed during training. We compare the pixel-wise and texture-wise accuracy of this 8-way, float32-bit GLCM with an offset of 2px to that of ImReN2UNET -MSE (trained without an intermediate loss function) and ImReN2UNET -VGG, and we use it as a replacement for the VGG function during training. As seen in Fig.8, the overall texture accuracy is also enhanced as compared to ImReN2UNET -VGG, using the 8-way, 4-bit GLCM metric from the previous section. Relative to variants using MSE-only and VGG as loss functions, ImReN2UNET-GLCM achieves better overall pixel-wise and texture-wise accuracy. Besides its potential use as a quality measure for texture recovery, the possibility to directly employing the GLCM as an unbiased loss function is an additional advantage.

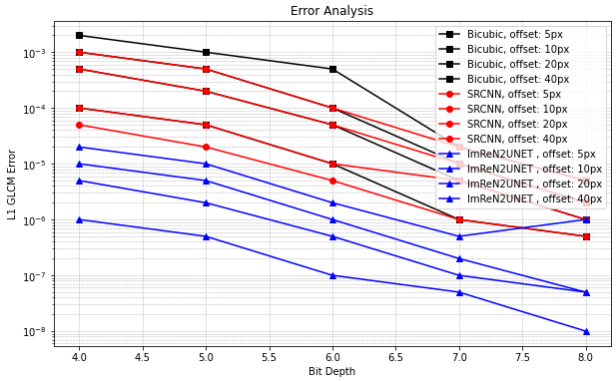

Fig.8. There is a consistent cardinal connection in terms of spatial texture reconstruction accuracy for various Images regardless of the bit depths and offset lengths used by the L1 GLCM

Table.3. Ablation experiment Result on Different input Sequences

MRI sequences	nFPC	sSens	Sens	DC	Prec
FLAIR only	0.615 ± 1.129	0.628	0.335 ± 0.312	0.285 ± 0.296	0.293 ± 0.284

T1 only	1.000 ± 1.109	0.629	0.308 ± 0.299	0.196 ± 0.157	0.328 ± 0.365
T1&FLAIR	0.163 ± 0.295	0.858	0.531 ± 0.337	0.395 ± 0.254	0.564 ± 0.286

Table.4. Ablation experiment Result on Different Self Attention Mechanism

Self-attention modules	nFPC	sSens	Prec	Sens	DC
CSA	0.858 ± 0.695	0.864	0.468 ± 0.378	0.567 ± 0.685	0.421 ± 0.218
SSA	0.727 ± 0.768	0.934	0.556 ± 0.385	0.587 ± 0.327	0.429 ± 0.348
DSA	0.159± 0.297	0.928	0.537 ± 0.397	0.438 ± 0.309	0.512 ± 0.397

Table.5. Ablation Study on Different Patch Size

Patch size	nFPC	sSens	Prec	Sens	DC
64^3	6.198 ± 2.945	0.864	0.316 ± 0.297	0.497 ± 0.318	0.465 ± 0.358
96^3	2.684 ± 1.842	0.894	0.379 ± 0.215	0.456 ± 0.425	0.428 ± 0.368
128^3	0.156 ± 0.297	0.918	0.528 ± 0.468	0.512 ± 0.496	0.518 ± 0.299

Table.6. Comparing the performance of the ImReN2UNET network as trained using MSE, MSE+VGG, and MSE+GLCM on the FCD dataset, both pixel-wise (higher is better) and texture-wise (lower is better)

Validation Images		
Model	**Mean PSNR (dB)**	**Mean L1-GLCM**
ImReN2UNET-MSE	35.4587	3.128e-4
ImReN2UNET-VGG	35.1289	2.648e-4
ImReN2UNET-GLCM	35.9725	2.098e-4

According to Table.6, the trained networks provide an average pixel-wise and texture-wise error, indicating that ImReN2UNET -GLCM delivers the best overall outcome. In contrast to the ImReN2UNET -VGG findings, which use the VGG loss function, the ImReN2UNET -MSE results are acquired without any intermediary loss function that would direct the production of SR images. It is important to mention that our auxiliary VGG model was trained to identify colored image elements instead of traditional greyscale X-ray textures. Therefore, ImReN2UNET -VGG exhibits the maximum level of pixelwise distortion. The biggest texture-wise error is shown in ImReN2UNET -MSE findings because the GAN-led creation of perceptually correct features is completely unguided and chaotic. Since ImReN2UNET -GLCM does not introduce any additional distortion to the pixel-wise setup, it can achieve a higher PSNR, making it more robust than ImReN2UNET -MSE and ImReN2UNET -VGG. Simultaneously, ImReN2UNET -GLCM enhances texture accuracy by bettering the spatial precision of pixel values.

5. CONCLUSION AND FUTURE SCOPE

The unknowable meaning of focal cortical dysplasia mainly stemmed out of the intricate texture and intensity values, which rendered the segmentation of lesions difficult. The newly developed ImReN2UNET model enhanced the emergent nn-U-Net by integrating a GLCM loss function into the newer and robust nn-U-Net architecture to address the challenges discussed. Thus, with texture knowledge advanced in deep learning, a remarkable increase in segmentation accuracy for FCD-lesions occurs. First, since the GLCM loss function is directly a strong metric for guiding the segmentation process, yet is not easily comprehended by traditional approaches, it allows the network to centre upon the essential texture features. Secondly, inner residual block architectures synergistically enhance the level of feature refinement. Its direct combination with nn-U-Net ensures good generalizability and competence across different datasets and imaging techniques. Due to the clear and sTable.segmentation results of FCD lesions by ImReN2UNET, the diagnostic capability and precision of treatment planning have increased, allowing a paradigm change in clinical practices. From the experiments conducted in the benchmark FCD datasets, the ImReN2UNET seems to be a step ahead of nn-U-Net regarding the segmentation concerning an increase of the Dice Similarity Coefficient from 98.79%. With the new GLCM-based loss function, an enhancement model was able to deliver better results related to small lesions by allowing the model to increase sensitivity to 99.67% concerning variation in texture. The model showed an impressive reduction of 96% in standard deviation in DSC scores signifying great variability in Dice scores across datasets. Further extensions would include further validation and potentially in the future, adapting the framework to other applications in the work field wherein texture application is through medical imaging.

REFERENCES

[1] R.D. Thijs, R. Surges, T.J.O'Brien and J.W. Sander, "Epilepsy in Adults", *The Lancet*, Vol. 393, pp. 689-701, 2019.

[2] I. Blumcke, R. Spreafico and G. Haaker, "Histopathological Findings in Brain Tissue Obtained during Epilepsy Surgery", *New England Journal of Medicine*, Vol. 377, pp. 1648-1656, 2017.

[3] K. Wagstyl, K. Whitaker and A. Raznahan, "Atlas of Lesion Locations and Postsurgical Seizure Freedom in Focal Cortical Dysplasia: A MELD Study", *Epilepsia*, Vol. 63, pp. 61-74, 2022.

[4] P. Widdess-Walsh, B. Diehl and I. Najm, "Neuroimaging of Focal Cortical Dysplasia", *Journal of Neuroimaging*, Vol. 16, pp. 185-196, 2006.

[5] L. Tassi, N. Colombo and R. Garbelli, "Focal Cortical Dysplasia: Neuropathological Subtypes, EEG, Neuroimaging and Surgical Outcome", *Brain*, Vol. 125, pp. 1719-1732, 2002.

[6] A.K. Nugroho, Afiahayati, M.E. Wibowo, H. Soebono and R. Wardoyo, "Skin Lesion Segmentation using Adaptive Color Segmentation and Decision Tree", *Journal of Wireless Mobile Networks, Ubiquitous Computing and Dependable Applications*, Vol. 15, No. 3, pp. 109-124, 2024.

[7] F. Isensee, P.F. Jager, P.M. Full, P. Vollmuth and K.H. Maier-Hein, "nnU-Net for Brain Tumor Segmentation", *Proceedings of International Workshop on MICCAI Brainlesion*, Vol. 12659, pp. 118-132, 2020.

[8] G. Litjens, T. Kooi and B.E. Bejnordi, "A Survey on Deep Learning in Medical Image Analysis", *Medical Image Analysis*, Vol. 42, pp. 60-88, 2017.

[9] L. Liu, J. Cheng, Q. Quan, F.X. Wu, Y.P. Wang and J. Wang, "A Survey on U-Shaped Networks in Medical Image Segmentation", *Neurocomputing*, Vol. 409, pp. 244-258, 2020.

[10] O. Ronneberger, P. Fischer and T. Brox, "U-Net: Convolutional Networks for Biomedical Image Segmentation", *Proceedings of International Workshop on MICCAI*, pp. 234-241, 2015.

[11] N. Siddique, S. Paheding, C.P. Elkin and V. Devabhaktuni, "U-Net and its Variants for Medical Image Segmentation: A Review of Theory and Applications", *IEEE Access*, Vol. 9, pp. 82031-82057, 2021.

[12] H. Najm, M.S. Mahdi and W.R. Abdulhussien, "Lightweight Image Encryption using Chacha20 and Serpent Algorithm", *Journal of Internet Services and Information Security*, Vol. 14, No. 4, pp. 436-449, 2024.

[13] T. Thesen, B.T. Quinn and C. Carlson, "Detection of Epileptogenic Cortical Malformations with Surface-based MRI Morphometry", *PLoS One*, Vol. 6, pp. 1-7, 2011.

[14] Z.I. Wang, S.E. Jones and Z. Jaisani, "Voxel-based Morphometric MRI Post-Processing in MRI-Negative Epilepsies", *Annals of Neurology*, Vol. 77, pp. 1060-1075, 2015.

[15] D.W. Praveenraj, T. Prabha, M. Kalyan Ram, S. Muthusundari and A. Madeswaran, "Management and Sales Forecasting of an E-Commerce Information System using Data Mining and Convolutional Neural Networks", *Indian Journal of Information Sources and Services*, Vol. 14, No. 2, pp. 139-145, 2024.

[16] M. El Azami, A. Hammers and J. Jung, "Detection of Lesions Underlying Intractable Epilepsy on T1-Weighted MRI as an Outlier Detection Problem", *PLoS One*, Vol. 11, pp. 1-7, 2016.

[17] D. David, J. Kroll-Seger and F. Schuch, "External Validation of Automated Focal Cortical Dysplasia Detection using Morphometric Analysis", *Epilepsia*, Vol. 62, pp. 1005-1021, 2021.

[18] B. Jin, B. Krishnan and S. Adler, "Automated Detection of Focal Cortical Dysplasia Type II with Surface-based MRI Post-Processing and Machine Learning", *Epilepsia*, Vol. 59, pp. 982-992, 2018.

[19] K. Wagstyl, S. Adler and B. Pimpel, "Planning Stereoelectroencephalography using Automated Lesion Detection", *Epilepsia*, Vol. 61, pp. 1406-1416, 2020.

[20] H. Spitzer, M. Ripart and K. Whitaker, "Interpretable Surface-based Detection of Focal Cortical Dysplasias", *Brain*, Vol. 145, pp. 3859-3871, 2022.

[21] X. Chen, X. Wang and K. Zhang., "Recent Advances and Clinical Applications of Deep Learning in Medical Image Analysis", *Medical Image Analysis*, Vol. 79, pp. 1-8, 2022.

[22] L. Walger, S. Adler and K. Wagstyl, "Artificial Intelligence for the Detection of Focal Cortical Dysplasia", *Epilepsia*, Vol. 64, pp. 1093-1112, 2023.

[23] H. Wang, S.N. Ahmed and M. Mandal, "Automated Detection of Focal Cortical Dysplasia using a Deep Convolutional Neural Network", *Computerized Medical Imaging and Graphics*, Vol. 79, pp. 1-9, 2020.

[24] R.S. Gill, S.J. Hong and F. Fadaie, "Deep Convolutional Networks for Automated Detection of Epileptogenic Brain Malformations", *Proceedings of International Conference on MICCAI*, pp. 490-497, 2018.

[25] R.S. Gill, H.M. Lee and B. Caldairou, "Multicenter Validation of a Deep Learning Detection Algorithm for Focal Cortical Dysplasia", *Neurology*, Vol. 97, pp. 1571-1582, 2021.

[26] J. Schlemper, O. Oktay and M. Schaap, "Attention-Gated Networks: Learning to Leverage Salient Regions in Medical Images", *Medical Image Analysis*, Vol. 53, pp. 197-207, 2019.

[27] A.K. Nugroho, R. Wardoyo, M.E. Wibowo and H. Soebono, "Thresholding Segmentation of Skin Lesions with Modified Ant Colony Optimization", *Journal of Wireless Mobile Networks, Ubiquitous Computing and Dependable Applications*, Vol. 15, No. 2, pp. 226-239, 2024.

[28] K.M.B. Dev, P.S. Jogi and S. Niyas, "Automatic Detection of Focal Cortical Dysplasia Lesions in MRI using Fully Convolutional Neural Network", *Biomedical Signal Processing and Control*, Vol. 52, pp. 218-225, 2019.

[29] S. Niyas, S.C. Vaisali and I. Show, "Segmentation of Focal Cortical Dysplasia Lesions from MRI using 3D CNNs", *Biomedical Signal Processing and Control*, Vol. 70, pp. 1-7, 2021.

[30] E. Thomas, S.J. Pawan and S. Kumar, "Multi-Res-Attention UNet for Segmentation of Focal Cortical Dysplasia", *IEEE Journal of Biomedical and Health Informatics*, Vol. 25, pp. 1724-1734, 2021.

[31] W. Assegid and G. Ketema, "Harnessing AI for Early Cancer Detection through Imaging and Genetics", *Clinical Journal for Medicine, Health and Pharmacy*, Vol. 1, No. 1, pp. 1-15, 2023.

[32] H. Dong, G. Yang, F. Liu, Y. Mo and Y. Guo, "Automatic Brain Tumor Detection and Segmentation using U-Net based FCNs", *Medical Image Understanding and Analysis*, pp. 506-517, 2017.

[33] A. Myronenko, "3D MRI Brain Tumor Segmentation using Autoencoder Regularization", *Proceedings of International Conference on Computer Vision and Pattern Recognition*, pp. 1-10, 2018.

[34] F. Isensee, P. Kickingereder, W. Wick, M. Bendszus and K.H. Maier-Hein, "Brain Tumor Segmentation and Radiomics Survival Prediction", *Proceedings of International Conference on Computer Vision and Pattern Recognition*, pp. 1-11, 2018.

[35] H. Li, A. Li and M. Wang, "A Novel End-to-End Brain Tumor Segmentation Method using Improved FCNs", *Computers in Biology and Medicine*, Vol. 108, pp. 150-160, 2019.

[36] Y.X. Zhao, Y.M. Zhang and C.L. Liu, "Bag of Tricks for 3D MRI Brain Tumor Segmentation", *Brainlesion (LNCS)*, pp. 210-220, 2020.

[37] K. He, X. Zhang, S. Ren and J. Sun, "Deep Residual Learning for Image Recognition", *Proceedings of*

International Conference on Computer Vision and Pattern Recognition, pp. 770-778, 2016.

[38] N. McConnell, A. Miron, Z. Wang and Y. Li, "Integrating Residual, Dense and Inception Blocks into the nnU-Net", *Proceedings of International Symposium on Computer-based Medical Systems*, pp. 217-222, 2022.

[39] J. Schlemper, O. Oktay and M. Schaap, "Attention-Gated Networks", *Medical Image Analysis*, Vol. 53, pp. 197-207, 2019.

[40] S. Niyas, S.C. Vaisali and I. Show, "Segmentation of Focal Cortical Dysplasia Lesions using 3D CNNs", *Biomedical Signal Processing and Control*, Vol. 70, pp. 1-7, 2021.

[41] E. Thomas, S.J. Pawan and S. Kumar, "Multi-Res-Attention UNet for Focal Cortical Dysplasia Segmentation", *Journal of Biomedical and Health Informatics*, Vol. 25, pp. 1724-1734, 2021.

[42] A. Hatamizadeh, Y. Tang and V. Nath, "UNETR: Transformers for 3D Medical Image Segmentation", *Proceedings of International Conference on Applications of Computer Vision*, pp. 574-584, 2022.

[43] A. Shaker, M. Maaz and H. Rasheed., "UNETR++: Delving into Efficient and Accurate 3D Medical Image Segmentation", *IEEE Transactions on Medical Imaging*, Vol. 43, No. 9, pp. 3377-3390, 2022.

[44] I.R. Haque and J. Neubert, "Deep Learning Approaches to Biomedical Image Segmentation", *Informatics in Medicine Unlocked*, Vol. 18, pp. 1-12, 2020.

[45] N. Ibtehaz and M.S. Rahman, "MultiResUNet: Rethinking the U-Net Architecture", *Neural Networks*, Vol. 121, pp. 74-87, 2020.

[46] A. Mechelli, C.J. Price, K.J. Friston and J. Ashburner, "Voxel-based Morphometry of the Human Brain", *Current Medical Imaging*, Vol. 1, pp. 105-113, 2005.

[47] P. Martin, G.P. Winston and P. Bartlett, "Voxel-based MRI Post-Processing in Epilepsy", *Epilepsia*, Vol. 58, pp. 1653-1664, 2017.

[48] O. Ronneberger, P. Fischer and T. Brox, "U-Net: Convolutional Networks for Biomedical Image Segmentation", *Proceedings of International Conference on Computer Vision and Pattern Recognition*, pp. 1-8, 2015.